New Consolidant-Hydrophobic Treatment by Combining SiO₂ Composite and Fluorinated Alkoxysilane: Application on Decayed Biocalcareous Stone from an 18th Century Cathedral

Dario S. Facio, Jose A. Ordoñez, M. L. Almoraima Gil, Luis A. M. Carrascosa and Maria J. Mosquera * [ID]

TEP-243 Nanomaterials Group, Department of Physical-Chemistry, Faculty of Sciences, Campus Río San Pedro, University of Cadiz, 11510 Puerto Real, Spain; dario.facio@uca.es (D.S.F.); joseantonio.ordonezperez@alum.uca.es (J.A.O.); almoraima.gil@uca.es (M.L.A.G.); luis.martinez@uca.es (L.A.M.C.)

* Correspondence: mariajesus.mosquera@uca.es; Tel.: +34-956-016331

check for updates

Abstract: An effective procedure has been developed to consolidate and hydrophobize decayed monumental stones by a simple sol-gel process. The sol contains silica oligomer, silica nanoparticles and a surfactant, preventing gel cracking. The effectiveness of the process on biocalcareous stone samples from an 18th century cathedral has been evaluated, and it was found that the gel creates effective linking bridges between mineral grains of the stone. Silica nanoparticles produced a significant increase in the mechanical resistance and cohesion of the stone. The application of an additional fluorinated oligomer onto the consolidated stone gave rise to a surface with lasting hydrophobicity, preventing water absorption.

Keywords: nanocomposite; consolidant; hydrophobic agent; *n*-octylamine; biocalcarenite; fluorine; cathedral

1. Introduction

Most stone building materials suffer significant weathering due to different processes such as salt crystallization, biodecay or carbonate cement dissolution, especially when exposed to outdoor conditions. All of these decay processes require water as a weathering agent carrier [1–3]. Susceptibility to deterioration of stone materials is mediated by several factors, including their mineral composition and their structural and textural properties. Stones—characterized by wide and highly accessible pores, such as biocalcareous stones—are especially susceptible to fast and intensive decay when exposed to a potentially aggressive environment [4].

Alkoxysilanes have been used with stone for restoration and conservation worldwide for decades [5]. The advantages of these products are well known: (1) alkoxysilanes penetrate deeply into porous stones, producing their polymerization in situ on the building, by a classic sol–gel process; (2) silica polymers with a silicon–oxygen backbone show good adherence to the stone, high weathering resistance and slight reduction of water vapor permeability. However, the alkoxysilanes have an important drawback associated with their tendency to crack. The presence of cracks obviously reduces their consolidant performance [6].

In the last years, we have prepared crack-free nanomaterials for stone conservation [7–18]. Specifically, the addition of an aqueous solution of *n*-octylamine to an alkoxysilane produces inverse micelles, which act as nanoreactors, generating silica seeds. These seeds grow, promoting a mesoporous

nanostructured xerogel [19]. As previously discussed [20], xerogel cracking is produced due to capillary pressure generated during the drying of the solvent contained in the pores of the gel network. Since this capillary pressure is inversely proportional to the pore radio, the obtained mesoporous xerogels (pore size from 2 to 20 nm) reduce this pressure, preventing cracking. In addition, the surfactant also reduces the capillary pressure by decreasing surface tension. By using this strategy, consolidants [7–12], hydrophobic and superhydrophobic products [10–13], stain-resistant materials [11] and photocatalytic coatings with self-cleaning performance [14–16] have been prepared. The interest in our approach is confirmed by the recent papers from other researchers working in the same field. Other authors [21–24] have employed the same route to produce protective materials for building. In addition, we have even applied our products in an actual cultural heritage building restoration. In recent papers [17,18], we described the restoration of a granitic Romanesque church and a medieval necropolis with a consolidant product synthesized in our laboratory.

In recent years, alkoxysilanes have also been modified in order to increase their mechanical resistance by adding colloidal oxide nanoparticles to the starting sol [6,25–29]. Nanoparticles are dense structures and, thus, they increase the mechanical properties and cohesion of the stone substrate. An increase of salt crystallization resistance of stone substrates treated with these particle-modified composites has been demonstrated [6]. Moreover, the addition of nanoparticles coarsens pore structure of the gel, preventing cracking [6,25].

Since water plays a significant role in building decay, hydrophobic products are commonly employed to prevent or reduce water ingress [11,12]. Specifically, organosilanes and organosiloxanes [11,12,30] and fluorinated compounds [1,31,32] are applied as conservation products on stone buildings because they reduce surface energy and thus produce a hydrophobic coating. Recently, superhydrophobic materials for building were produced [13,33] by adding silica nanoparticles to a low surface energy component. They produce a Cassie–Baxter surface, since air is trapped beneath the water droplets. This minimizes the contact area between droplet and surface, promoting repellence.

The starting point of this work was the restoring intervention on a stone altarpiece affected by efflorescence, superficial detachments and sand disaggregation from the Cathedral of Jerez de la Frontera in the south of Spain. The stone used in this construction easily undergoes weathering, mainly because of its high porosity. In particular, it suffers the weathering induced by salt crystallization, causing a considerable defacement and decohesion of the stone [4]. Thus, a treatment promoting consolidant and hydrophobic performance was applied [34]. A nanocomposite containing silica nanoparticles integrated into a silica matrix was produced. The nanoparticles were added (1) to increase the mechanical resistance of the coating and (2) to increase roughness of the surface in order to produce water repellence. A surfactant, *n*-octylamine, was added to the starting sol to prevent cracking and to act as a catalyst. This product was applied on biocalcareous stones employed in the construction of the Cathedral of Jerez de la Frontera. In addition, a second coating of fluorinated alkoxysilane was applied to produce condensation between labile silanol groups present in the silica nanocomposites and in the fluorinated coating. The objective was to produce a lasting coating, increasing mechanical resistance and giving high hydrophobicity to the stone substrate. The effectiveness for consolidant and hydrophobic purposes was evaluated. For comparison, commercial consolidant and hydrophobic products were also tested.

2. Materials and Methods

2.1. Description of the Monumental Building Stone

The building stone of the Cathedral of Jerez de la Frontera is a biocalcarenite from the San Cristobal quarry located in the southwest of Spain (see map in Figure 1) that has been employed in numerous emblematic monumental buildings in Spain's southwest region, such as the Cathedral of Seville and the Cathedral of Cádiz. It is a yellow-cream stone mainly containing calcite ($\approx$45%) and quartz ($\approx$45%) and a low content in feldspar ($\approx$10%). The mercury accessible porosity value is around 35%.

Figure 1. Geographical location of the San Cristobal Quarry and the Cathedral of Jerez de la Frontera. The biocalcareous stone under study is shown in the inset.

2.2. Consolidant and Hydrophobic Products and Application Procedure

The following treatments were selected for testing.

UCA (from the University of Cádiz) treatments. Starting sols were prepared by mixing a silica oligomer, *n*-octylamine and silica nanoparticles. Wacker TES40 (TES40, Wacker Chemie, Munich, Germany) is a mixture of monomeric and oligomeric ethoxysilanes, with an average chain length of approximately five Si–O units. Aerosil OX50 (OX50, Evonik Industries, Essen, Germany) is hydrophilic fumed silica with an average particle diameter of 40 nm.

The nanomaterial was prepared as follows: (1) an aqueous dispersion of *n*-octylamine, with a significantly higher surfactant concentration than that corresponding to its critical micellar concentration (cmc), was prepared under vigorous stirring. Specifically, a 1.92 M aqueous dispersion of *n*-octylamine was employed; (2) TES40 and OX50 were mixed under ultrasonic stirring (2 W·cm^{-3}) during 1 min; (3) the aqueous dispersion of *n*-octylamine was added dropwise to the TES40/OX50 mixture under ultrasonic stirring (1 W·cm^{-3}). The ultrasonic agitation was maintained for 8 min. The TES40/*n*-octylamine dispersion ratio was 99.5/0.5 *v/v*. The OX50 was added in 2% *w/v* ratio with respect to the total volume of the sol. The nomenclature for this nanomaterial is TS (T for TES40 and S for OX50). For comparison purposes, we also prepared a nanomaterial without the silica colloidal particles by using the same procedure, named T.

These sols were applied by air spraying at 2.0 bar for 5 s on the upper surface of $4 \times 4 \times 4 \, cm^3$ stone sample cubes, in triplicate. Spraying was chosen as the method of application because it is the preferred procedure employed, in real situations, for large areas, such as buildings or monumental structures. The application was repeated five times with an elapsed time of 1 min to ensure the saturation of all products under study and, thus, the suitable sol penetration into the stone. The products were applied under laboratory conditions (20 °C, 45% RH).

After gel transition took place (2 days after application), a perfluoropolyether silane solution (FS10, Fluorolink S10, Solvay Solexis, West Deptford, NJ, USA) was applied to the stone samples. Prior to its application, it was subjected to acid-catalyzed hydrolysis according to the following procedure: FS10 was mixed with isopropanol, H$_2$O and acetic acid under magnetic stirring. The proportions of the reagents were: 1.0, 94.0, 4.0 and 1.0 wt %, respectively. The fluorinated coating was applied by air spraying at 2.0 bar for 3 s. Finally, the coating was subjected to heating in order to accelerate the polymerization process, at two different temperatures: (1) 100 °C for 15 min and (2) 120 °C for 15 min. According to the technical data sheet, heating is not strictly necessary; room temperature curing is

also possible, but this will lead to a longer time to achieve the final performance. Treatments with the fluorinated layer have the additional keyword "+F" added to their name.

For comparative purposes, a commercial consolidant, Tegovakon V100 (TV100, BASF, Ludwigshafen, Germany), and a hydrophobic product, SILRES BS 290 (BS290, Wacker Chemie, Munich, Germany), were also applied on stone samples. TV100 is a solvent-free one-component consolidant consisting of partially prepolymerized TEOS and dioctyltin dilaurate (DOTL) catalyst. BS290 is a solvent-free silane/siloxane mix with application as a hydrophobic treatment. Following the specifications of the manufacturer, BS290 was diluted in ethanol (12 wt %). The two commercial products were applied by using the same procedure as UCA products.

2.3. Effectiveness Evaluation on Biocalcareous Stone

2.3.1. Effectiveness on Quarry Stone

One month after the application of the products, the evaluation tests described in the following paragraph were carried out. Results are expressed as average values with their standard deviations. In the cases in which the fluorinated coating did not influence the obtained results, these results are not shown in order to prevent duplication of data.

The uptake and dry matter of the products on the stone substrate were evaluated. The uptake of the consolidants was calculated by the difference in weight, expressed in wt %, after and before the treatment. The content of dry matter was determined by difference in weight of the samples left to dry under laboratory conditions until reaching constant weight, expressed in wt %.

Surface fragments of the treated stone specimens and their untreated counterparts were visualized by scanning electron microscopy (SEM) using a JEOL Quanta 200 scanning electron microscope (Tokyo, Japan) in order to observe the distribution and morphology of the coatings on the surface of the biocalcarenite stone.

Mercury accessible porosity and the porosimetric distribution by mercury intrusion porosimetry (MIP) was carried out. The test was carried out on stone specimens from the treated surfaces, each with a surface around 2 cm^2 and a width of around 0.5 cm, in triplicate. In the case of the untreated stone sample, the specimens were collected from any face. A PoreMaster 60 device from Quantachrome Instruments, which generates pressure to 60,000 psia, was used for pore size analysis from 950 to 0.0036 μm pore diameter.

Improvement in mechanical properties of the treated stones was evaluated by using a drilling resistance measurement system (DRMS) [35] by SINT Technology (Calenzano, Italy). Drill bits with 4.8 mm diameter were employed with a rotation speed of 600 rpm and a penetration rate of 10 mm/min. The test was repeated on two samples for each treatment, and five holes were drilled in each specimen. Drilling resistance vs. testing depth profiles were obtained.

The effectiveness of the coating materials in providing hydrophobic protection was characterized by measurement of the contact angles according to the sessile drop method, using a commercial, video-based, software-controlled contact angle analyzer, model OCA 15 plus from Dataphysics Instruments (Filderstadt, Germany). Static contact angle values were determined on the stone surface. For each treatment evaluated, droplets of distilled water (10 μL) were applied by a needle to five different points on two different stone samples. The advancing and receding contact angles were measured using the ARCA (Advancing and Receding Contact Angles) method included in the equipment software (OCA 15 plus), with the volume of the droplet being increased/decreased by 5 μL. Details of this procedure are given in a previous paper [10].

To confirm the hydrophobic behavior of the materials, two stone samples for each treatment were subjected to a test of water absorption by capillarity (WAC), as recommended in UNE-EN 1925 [36].

We also evaluated the possible negative effects, such as color changes and reduction in vapor permeability, induced by the treatments.

Water vapor permeability was determined by means of an automatic setup developed in our laboratory [37], based on the standard cup test [38], on $4 \times 4 \times 1$ cm^3 stone slabs. Two samples were tested for each treatment.

Total color difference (ΔE^*) was determined using a solid reflection spectrophotometer, Colorflex model, from HunterLab (Reston, VA, USA). The conditions used were illuminant C and observer CIE 10°. CIE $L^*a^*b^*$ scale was used, and variations in color were evaluated [39]. In this case, the color evaluation was carried out after two different elapsed times from the treatment applications: 1 month and 1 year.

2.3.2. Effectiveness on Monumental Stone Extracted from Jerez de la Frontera Cathedral

The most effective treatment, identified in the previous phase, was applied to samples obtained from a restoration intervention on a stone altarpiece of the Cathedral of Jerez de la Frontera in the southwest of Spain (Figure 2a). The building construction began in 1695 and was inaugurated in 1778. The long duration of the construction works of the Cathedral means that three architectural styles can be found in the Cathedral: Neoclassical, Baroque and Gothic [4]. The altarpiece is affected by efflorescence, superficial detachments and sand disaggregation, as can be observed in Figure 2b,c. A stone fragment removed from the altarpiece was cut in a similar way to those collected from San Cristobal quarry ($4 \times 4 \times 4$ cm^3 stone sample cubes, see Figure 1).

Figure 2. (**a**) View of the main facade of the Cathedral of Jerez de la Frontera. (**b**) Stone altarpiece of the Cathedral from which samples were obtained. (**c**) Detail of the stone altarpiece affected by efflorescence, superficial detachments and sand disaggregation.

The treatment was applied by spraying in the same manner as that used for the quarry samples. One month after the treatment, the following experiments were carried out on those samples.

A peeling test was carried out, according to previously reported methods [40,41], using Scotch Magic tape (3M, Maplewood, MN, USA). Three strips of tape were applied and removed consecutively from the stone surface, and the weight of material pulled off in each stripping was recorded.

In addition, the drilling resistance test, water contact angle evaluation, water absorption by capillarity and measurement of color were carried out according the procedures described in the previous section.

3. Results and Discussion

3.1. Evaluation of the Effectiveness on Quarry Stone

Table 1 shows the uptake and dry matter (DM/U) values for the products. Uptake of the products ranged from 3 to 6 wt % in all cases. The dry matter values show a significantly lower value for BS290, its evaporated mass being around 87%. On the other hand, the higher DM/U values observed for the UCA products than those associated with TV100 highlights a slower gel drying.

Table 1. Uptake, dry matter and percentage relationship between dry matter and uptake (DM/U) after the application of the treatments under laboratory conditions.

Treatment	Uptake (%)	Dry Matter (%)	DM/U (%)
TV100	5.70 ± 2.93	3.17 ± 1.43	56
BS290	4.41 ± 2.24	0.58 ± 0.24	13
UCA-T	5.63 ± 1.19	4.11 ± 0.63	73
UCA-TS	5.65 ± 0.72	4.46 ± 0.58	79
UCA-T+F	5.59 ± 0.60	3.97 ± 0.33	71
UCA-TS+F	5.71 ± 0.17	4.10 ± 0.17	72

This finding demonstrates that, in the case of BS290, which was dissolved in ethanol, a thin film is formed on the stone substrate due to the solvent evaporation. It can be observed that the higher DM/U relationship for the UCA treatments is because volatile organic compounds were not added in the synthesis process. In the case of products containing fluorine, no differences from their counterparts without F are observed. This is due to the fluorine being applied in alcoholic solution (90%). We want to highlight that the purpose of this product application is exclusively to functionalize the UCA consolidants previously applied in order to reduce their surface energy and, subsequently, to promote a hydrophobic performance.

Figure 3 shows the SEM micrographs of the stone specimens with the treatments under study and their untreated counterparts. The untreated biocalcarenite reveals the presence of quartz and calcite crystals, typical of this stone (Figure 3a). The stone consolidated with TV100 shows the formation of a dense gel coating severely affected by cracking produced during its drying onto the stone (Figure 3b). Cracking is generated by the high capillary pressures supported by the gel network during drying, which is due to the presence of micropores [7,9], and gel network stiffness promoting cracking. The BS290 coating (Figure 3c) results in a dense and non-particulated polymer matrix due to the gel network compliance, promoting the pores' collapse. The gel compliance is produced by the presence of organic components in the network, as previously described [42]. In contrast, the samples consolidated with UCA-T and UCA-TS present particulated, continuous, homogeneous and crack-free coatings (Figure 3d,e, respectively). We associate particle formation to the role of *n*-octylamine producing inverse micelles that act as nanoreactors, as discussed in the Introduction section [19]. By comparing the two UCA products, the UCA-TS (Figure 3e) coating presents a more particulate texture as a result of the addition of commercial colloidal silica particles into the material. Specifically, the commercial silica particles are aggregated to the silica particles created during sol–gel transition, producing SiO_2 matrix–SiO_2 nanoparticle aggregates of around 240 nm. Thus, larger and more defined particle aggregates are created than those corresponding to the coating without OX50 particles. These micrographs highlight that the novel materials prevent cracking. Figure 4 shows some UCA-TS bridges linking the quartz grains and, consequently, confirming the effective consolidation produced by our products [7,9]. Furthermore, UCA-TS material homogeneously covers the edged surface of the quartz grains.
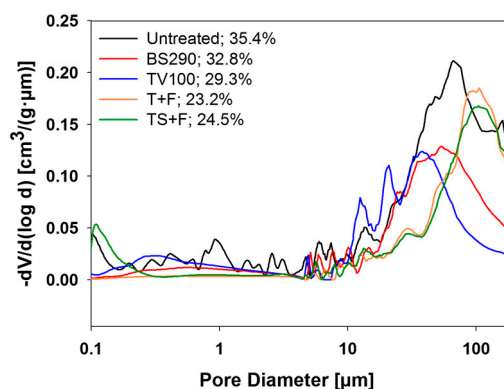
Figure 5 shows the porosity values and the pore size distributions. After products' application, porosity was reduced in all cases, showing a clear relationship with dry matter values. UCA treatments (T and TS), showing the greatest DM/U proportion values in all cases, produce the greatest reduction in the stone porosity. On the other hand, the commercial treatments are those with the lowest reduction of porosity, with nearly similar values of total porosity (TP), related to their lower DM/U values. The lowest reduction is produced in the samples treated with BS290, because a thin film is produced.
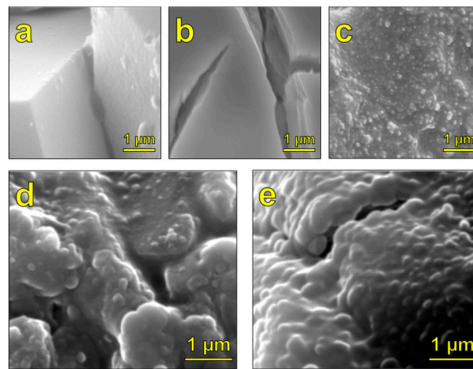
Figure 3. Scanning electron microscopy micrographs of the biocalcareous stone under study: (**a**) untreated; (**b**) treated with TV100; (**c**) treated with BS290; (**d**) treated with UCA-T; and (**e**) treated with UCA-TS.
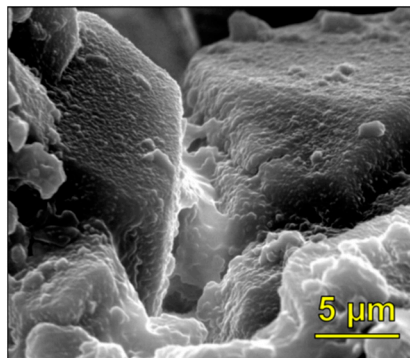
Figure 4. Scanning electron microscopy micrograph of the biocalcareous stone treated with UCA-TS. Nanomaterial bridges linking the quartz grains of the stone together can be clearly observed.


Figure 5. Pore size distribution obtained by mercury intrusion porosimetry (MIP) of the treated biocalcarenite samples and their untreated counterpart. Total porosity values (%) are also included after the corresponding treatment legend.

Comparing the pore size distribution, it is observed that all the treatments reduce the percentage of pores with larger access diameter (>10 μm), whereas the intermediate porosity (1–10 μm) was either increased or maintained in the case of the commercial products, and was reduced after application of UCA products. In the case of the smallest pores, the UCA treatments completely filled the micropores (<1 μm). The disappearance of the smallest pores is an important feature because salt crystallization, which is a damage mechanism in biocalcareous stone, is produced in micropores [17,43].

The consolidant effect of the products on the biocalcareous stone was measured by drilling resistance (see Figure 6). The stones treated with BS290 were not evaluated because it is not a consolidant. The commercial consolidant hardly has consolidant effectiveness on the biocalcareous stone, whereas the stone samples treated with the products synthesized in our laboratory significantly increased the mechanical resistance. This feature occurs because UCA products do not crack inside the porous structure of the stone, and they create effective links between the grains of the stone material, improving its cohesion (Figure 4). The increase in the mechanical resistance of the stone was evident across the full depth of stone tested (40 mm), demonstrating that our products penetrate deeply into the stone structure and they act as effective consolidants. In the case of TV100, its poor effectiveness is associated with the formation of a completely cracking coating (see Figure 3b).

By comparing the two UCA products, it can be observed that the stone treated with the particle-modified product shows a significantly higher mechanical resistance, being improved by a factor of around 1.5, 2 and 5 related to UCAT, TV100 and the untreated sample, respectively. This confirms the role played by the nanoparticles in increasing the consolidant effect of the product, as previously reported by other authors [6,26–29].
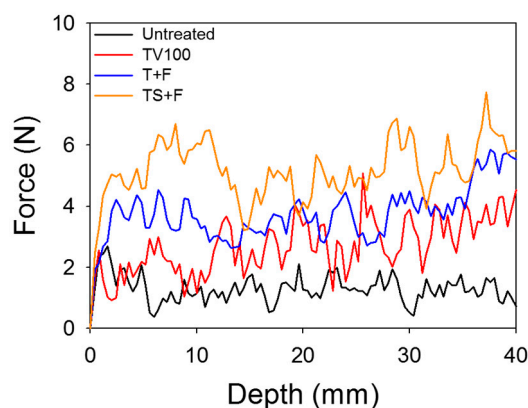
Figure 6. Drilling resistance versus testing depth of treated stone samples and their untreated counterpart.

Figure 7 and Table S1 show water droplet static and dynamic contact angle (CA) values. In the case of the untreated stone, due to its high porosity and hydrophilic nature, it was impossible to measure its CAs because the water was quickly absorbed. Comparing between treatments, the samples of stone treated with the commercial product TV100 present the lowest contact angles, which are below 90°. This is because TV100 is not a hydrophobic product and, subsequently, low surface energy groups are not present on the stone surface. The stones treated with UCA-T and UCA-TS show receding CA values below 90°, but advancing and static CA are above this value, in spite of groups reducing surface energy not being included in these products. We associate these anomalously high CA values with the incomplete hydrolysis of the ethoxy groups from the silica oligomer. This effect is not supposed to persist over time due to the progress of the hydrolysis reaction in both cases. This feature has been confirmed by the ^{29}Si-NMR spectra obtained for gels containing *n*-octylamine in a previous paper [12]. "The products containing *n*-octylamine presented Q1 and Q2 units in conjunction with Q3 and Q4 species six months after the synthesis, which indicated that the silica is not completely condensed and consequently, some ethoxy groups could be present in the material", as previously described [12,44]. However, the TV100 ^{29}Si-NMR spectrum does not show Q1 and Q2 units. The absence of the peaks highlights that ethoxy groups are not present in the TV100 gel and, consequently, the CA values are lower than 90°, as observed in this work (see Figure 7). By comparing CA values obtained in samples treated with UCA-T and UCA-TS, similar values are obtained, showing a slight increase for the gel containing silica nanoparticles. This can be related to the increase in roughness produced by particles in the surface of the stone [13,33].
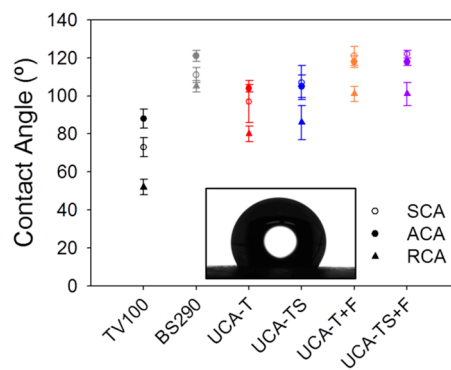
Figure 7. Static contact angle (CA) values and their corresponding advancing and receding CAs for the treated stones. Inset image corresponds to a droplet on stone with TS + F treatment.

Regarding the samples treated with products containing low energy species (BS290, UCA-T + F and UCA-TS + F), significantly higher CA values were obtained, presenting receding CA values higher than 90°. Thus, all treatments can be considered hydrophobic due to the presence of low energy components (fluorinated species) [45]. Comparing the treatments shows that the CA values are similar, with static CA values being slightly higher for UCA products. The silica nanoparticles were added, apart from improving its mechanical properties, to produce a densely packed coating in which the air is trapped. Thus, its addition should promote the movement of water droplets across the surface (repellence), producing a Cassie–Baxter state [46]. This regime is associated with a low CA hysteresis, below 10°. However, the surface treated with the product with nanoparticles (UCA-TS + F) shows the same hysteresis value (17°) as that corresponding to the treatment without particles (UCA-T+F) and, consequently, the repellence effect is not achieved. Since repellence is related to the change produced in the topography of the surfaces, SEM images (see Figure 3) allow this behavior to be explained. When SiO_2 nanoparticles are integrated into the silica gel, they cause clear and visible morphological changes in the coating due to the formation of larger aggregates (see Figures 3 and 4). However, this change does not produce modifications in repellence behavior because the original topography of the stone surface is hardly modified by the coating (see Figure 4). Consequently, as the biocalcareous stone is a high porosity material composed of macropores with distance between roughness peaks in the micrometer range, and a significantly lower distance between roughness peaks in the nanometer range is required to produce a Cassie–Baxter regime [13,33,47]. The coating containing nanoparticles (UCA-TS) cannot produce a repellent surface on which the water droplets do not stick [48]. These high pitch values promote a Wenzel surface [33,48]. In this scenario, water penetrates into the grooves and valleys of roughness, promoting a high adhesion [49].

In order to corroborate the hydrophobicity produced by the materials under study, a water absorption by capillarity (WAC) test was carried out on the stone samples under study. The WAC results are given in Table 2.

Table 2. Vapor diffusivity (*D*), total water uptake by capillarity (TWU) and total color difference (Δ*E**) for each treatment and its untreated counterpart. For each value of *D*, the percentage of reduction (DR) with respect to the untreated stone is also given.

Treatment	$D \cdot 10^{-6}$ (m$^2 \cdot$s^{-1})	DR (%)	TWU (%)	Δ*E** (1 Month)	Δ*E** (1 Year)
Untreated	−10.04 ± 2.12	–	15.31 ± 1.29	–	–
TV100	−7.03 ± 0.22	30	4.02 ± 0.01	2.12 ± 0.69	2.23 ± 1.33
BS290	−8.53 ± 0.36	15	0.48 ± 0.13	10.12 ± 2.11	6.03 ± 0.69
UCA-T	−6.95 ± 0.80	31	0.35 ± 0.10	10.59 ± 1.71	6.12 ± 1.69
UCA-TS	−6.21 ± 0.13	38	0.33 ± 0.00	11.16 ± 3.06	5.97 ± 2.27
UCA-T + F	−6.96 ± 1.12	31	0.22 ± 0.10	8.72 ± 0.81	4.76 ± 0.89
UCA-TS + F	−6.02 ± 0.04	40	0.20 ± 0.04	9.12 ± 0.78	4.91 ± 1.75

As expected, the stone samples treated with TV100 show a significant water uptake. The UCA treatments present the highest reduction in WAC, being significantly higher for those with the fluorine coating. Surprisingly, the commercial hydrophobic product (BS290) produced higher water absorption than that associated with non-hydrophobic UCA products. This could be related to the lower reduction in porosity produced by this coating (see Figure 5). This could favor the existence of pores enabling water absorption. In addition, we think that the existence of chemical bonds between the silica nanocomposite and the fluorine oligomer coating creates a lasting hydrophobic coating preventing water uptake, whereas the commercial hydrophobic product could produce a coating with lower durability for water uptake due to the formation of a discontinuous coating, as described in a previous paper [50].

Regarding the negative effect, we studied changes occurring in the water vapor permeability and in the color of the stone after the treatments. Water vapor diffusivity coefficients are given in Table 2. A treatment is not acceptable for restoration of stone materials if it causes a reduction of water vapor diffusivity coefficient (*D*) by more than 50% [51] because it suppresses the breathability (water vapor transference across the pore structure) of the stone. This critical value was not exceeded by any of the treatments evaluated; the lowest diffusivity reduction (DR) corresponded to the samples treated with BS290. This could be newly associated to the thin film created, producing a low reduction in porosity of the stone (see Figure 5).

To evaluate the color change produced by the treatments, the chromatic variations were quantified by the total color difference values (ΔE^*) (Table 2). All of the treatments, excepting TV100, presented total color difference values higher than the generally accepted threshold value of human eye perception ($\Delta E^* \leq 5$) 1 month after their application [26]. Change in color was evaluated 1 year after application (see Table 2), with all the stones treated showing ΔE^* values around the accepted threshold. Thus, we consider that change in color induced by the UCA products is acceptable for restoration purposes.

3.2. Effectiveness on Monumental Stone Extracted from Jerez de la Frontera Cathedral

Since the stonework of the Cathedral of Jerez de la Frontera is affected by salt decay, with water being the main vehicle for the decay agents, the choice of product with consolidant and hydrophobic performances is highly required. From the results of the tests performed on the biocalcarenite samples extracted from the quarry, we concluded that the UCA-TS + F treatment is the best product to be applied on the Cathedral stonework, as it showed the highest consolidant performance due to the SiO_2 nanoparticles added to the starting sol. Thus, this treatment was applied on stone samples obtained from the altarpiece of the Cathedral. Table 3 shows the values obtained for uptake, dry matter and total color variation. As expected, the results are very close to those obtained for the stone samples from the quarry.

Table 3. Uptake, dry matter and total color difference (ΔE^*) with respect to the untreated stone. Weight of the tape in the adhesion test is also given.

Treatment	Uptake (%)	Dry Matter (%)	ΔE^*	Adhesion Test (mg)
Untreated	–	–	–	9.3 ± 9.4
UCA-TS + F	4.83 ± 0.52	3.64 ± 0.40	10.65 ± 0.99	0.1 ± 0.2

As described in the introduction, stone samples from the altarpiece show evident superficial detachments and sand disaggregation. Therefore, the peeling test was used as a useful tool to confirm the superficial cohesive performance of the UCA-TS + F treatment. The results from the adhesion test (see Figure 8a and Table 3) show a significant amount of material released from the surface of the untreated stone due to significant decohesion. After the application of the UCA treatment, the material removal was negligible (see Figure 8b). These results highlight that this product has a potential use as consolidant of decayed stone with low cohesion, such as the biocalcareous monumental stone under study.
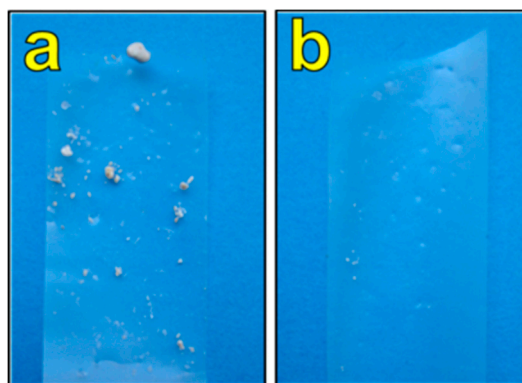
Figure 8. Scotch tape in the adhesion test for (**a**) untreated stone and (**b**) UCA-TS + F treated stone.

In addition to the increase in the cohesion of the external surface produced by the UCA product, a significant increase was observed in drilling resistance (see Figure 9), doubling the value of the untreated stone. Regarding the profile of the untreated stone, we observed a higher mechanical resistance than that obtained from the quarry stone. We associate this with variations in the mineral vein from which they were extracted.
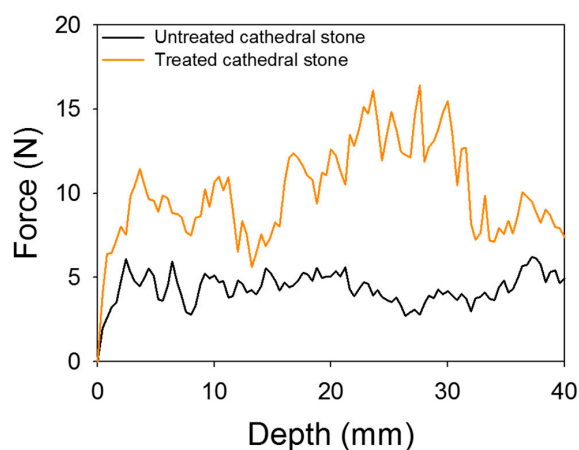
Figure 9. Drilling resistance versus testing depth of UCA-TS + F treated stone and its untreated counterpart.

Regarding the hydrophobic behavior of the treated monumental stone (see Table 4), the results for the effectiveness of the product were close to those obtained from the quarry stones, showing high contact angle values and low water uptake. This confirms the effectiveness of the UCA treatment in conferring hydrophobic properties to the decayed monumental stone.

Table 4. Static CA values and their corresponding advancing and receding CA for the treated stones, and total water uptake by capillarity (TWU).

Treatment	θ_S (°)	θ_A (°)	θ_R (°)	Hysteresis (°)	TWU (%)
Untreated	–	–	–	–	12.50
UCA-TS+F	123 ± 2	118 ± 1.13	101 ± 3	17.91 ± 1.97	0.19

Note: θ_S = Static contact angle; θ_A = advancing angle; θ_R = receding angle; TWU = total water uptake.

Finally, we would like to remark that, in spite of the stones extracted from the altarpiece containing salt efflorescence, the product prepared in our laboratory was effective as a consolidant and hydrophobic agent, showing similar results to those obtained for the quarry stones.

4. Conclusions

A simple procedure has been developed to consolidate decayed stone with low cohesion and evident sand disaggregation, such as the biocalcareous monumental stone under study. Specifically, a sol containing silica oligomer, silica nanoparticles and a surfactant is applied on stone by spraying. The process is so simple that the polymerization is produced in situ, and it can take place on a building in outdoor conditions. We demonstrated that a crack-free coating, filling pores of the decayed stone, was obtained due to the effect of *n*-octylamine. It acts by coarsening the pore structure of the material. The addition of silica nanoparticles to the starting sol produces a significant increase in mechanical resistance and in the cohesion of the stone. We demonstrated that the silica composite creates linking bridges between the mineral grains of the stone. This product shows higher consolidant effectiveness than that obtained from a commercial product tested in this study.

Additionally, the application of a fluorinated alkoxysilane onto the treated stone gives rise to a hydrophobic surface, preventing water absorption. The chemical bonds created between the two applied coatings (silica nanocomposite and fluorinated oligomer) produces a lasting hydrophobic coating, showing a higher reduction in uptake than that obtained by a commercial hydrophobic product tested. The addition of silica nanoparticles does not produce a Cassie–Baxter surface in this specific substrate due to the original topography of the stone surface being hardly modified by the coating. Thus, repellence properties are not achieved.

Finally, we demonstrated that the treatments do not significantly modify the breathability of stone and the color of the stone.

References

1. Poli, T.; Toniolo, L.; Chiantore, O. The protection of different Italian marbles with two partially flourinated acrylic copolymers. *Appl. Phys. A Mater. Sci. Process.* **2004**, *79*, 347–351. [CrossRef]
2. Graedel, T.E.; McGill, R. Degradation of materials in the atmosphere. *Environ. Sci. Technol.* **1986**, *20*, 1093–1100. [CrossRef]
3. Dolske, D.A. Deposition of atmospheric pollutants to monuments, statues, and buildings. *Sci. Total Environ.* **1995**, *167*, 15–31. [CrossRef]
4. Villegas-Sánchez, R.; Arroyo, F. The cathedral of Jerez De La Frontera (Cádiz, Spain): Stone degradation and conservation. *J. Cult. Herit.* **2013**, *14*, e113–e116. [CrossRef]
5. Wheeler, G. *Alkoxysilanes and the Consolidation of Stone*; The Getty Conservation Institute: Los Angeles, CA, USA, 2005.
6. Scherer, G.W.; Wheeler, G.S. Silicate consolidants for stone. *Key Eng. Mater.* **2009**, *391*, 1–25. [CrossRef]
7. Mosquera, M.J.; de los Santos, D.M.; Montes, A.; Valdez-Castro, L. New nanomaterials for consolidating stone. *Langmuir* **2008**, *24*, 2772–2778. [CrossRef] [PubMed]
8. Mosquera, M.J.; Desireé, M.; Valdez-Castro, L.; Esquivias, L. New route for producing crack-free xerogels: Obtaining uniform pore size. *J. Non-Cryst. Solids* **2008**, *354*, 645–650. [CrossRef]

9.   Mosquera, M.J.; de los Santos, D.M.; Rivas, T.; Sanmartín, P.; Silva, B. New nanomaterials for protecting and consolidating stone. *J. Nano Res.* **2009**, *8*, 1–12. [CrossRef]

10. Mosquera, M.J.; de los Santos, D.M.; Rivas, T. Surfactant-synthesized ormosils with application to stone restoration. *Langmuir* **2010**, *26*, 6737–6745. [CrossRef] [PubMed]

11. Illescas, J.F.; Mosquera, M.J. Surfactant-synthesized PDMS/silica nanomaterials improve robustness and stain resistance of carbonate stone. *J. Phys. Chem. C* **2011**, *115*, 14624–14634. [CrossRef]

12. Illescas, J.F.; Mosquera, M.J. Producing surfactant synthesized nanomaterials in situ on a building susbstrate, without volatile organic compounds. *ACS Appl. Mater. Interfaces* **2012**, *4*, 4259–4269. [CrossRef] [PubMed]

13. Facio, D.S.; Mosquera, M.J. Simple strategy for producing superhydrophobic nanocomposite coatings in situ on a building substrate. *ACS Appl. Mater. Interfaces* **2013**, *5*, 7517–7526. [CrossRef] [PubMed]

14. Pinho, L.; Mosquera, M.J. Titania-silica nanocomposite photocatalysts with application in stone self-cleaning. *J. Phys. Chem. C* **2011**, *115*, 22851–22862. [CrossRef]

15. Pinho, L.; Mosquera, M.J. Photocatalytic activity of TiO_2-SiO_2 nanocomposites applied to buildings: Influence of particle size and loading. *Appl. Catal. B Environ.* **2013**, *134–135*, 205–221. [CrossRef]

16. Pinho, L.; Rojas, M.; Mosquera, M.J. Ag–SiO_2–TiO_2 nanocomposite coatings with enhanced photoactivity for self-cleaning application on building materials. *Appl. Catal. B Environ.* **2015**, *178*, 144–154. [CrossRef]

17. De Rosario, I.; Elhaddad, F.; Pan, A.; Benavides, R.; Rivas, T.; Mosquera, M.J. Effectiveness of a novel consolidant on granite: Laboratory and in situ results. *Constr. Build. Mater.* **2015**, *76*, 140–149. [CrossRef]

18. De Rosario, I.; Rivas, T.; Buceta, G.; Feijoo, J.; Mosquera, M.J. Surfactant-synthesized consolidants applied to a granitic medieval necropolis in NW Spain. Laboratory and in situ effectiveness evaluation. *Int. J. Archit. Herit.* **2017**, *11*, 1166–1176. [CrossRef]

19. Facio, D.S.; Luna, M.; Mosquera, M.J. Facile preparation of mesoporous silica monoliths by an inverse micelle mechanism. *Microporous Mesoporous Mater.* **2017**, *247*, 166–176. [CrossRef]

20. Scherer, G. Theory of drying. *J. Am. Ceram. Soc.* **1990**, *73*, 3–14. [CrossRef]

21. Xu, F.; Yu, J.; Li, D.; Xiang, N.; Zhang, Q.; Shao, L. Solvent effects on structural properties of SiO_2 gel using *n*-octylamine as a catalyst. *J. Sol-Gel Sci. Technol.* **2014**, *71*, 204–210. [CrossRef]

22. Xu, F.; Li, D.; Zhang, Q.; Zhang, H.; Xu, J. Effects of addition of colloidal silica particles on TEOS-based stone protection using *n*-octylamine as a catalyst. *Prog. Org. Coat.* **2012**, *75*, 429–434. [CrossRef]

23. Simionescu, B.; Olaru, M.; Aflori, M.; Cotofana, C. Silsesquioxane-based hybrid nanocomposite with self-assembling properties for porous limestones conservation. *High Perform. Polym.* **2010**, *22*, 42–55. [CrossRef]

24. Simionescu, B.; Aflori, M.; Olaru, M. Protective coatings based on silsesquioxane nanocomposite films for building limestones. *Constr. Build. Mater.* **2009**, *23*, 3426–3430. [CrossRef]

25. Mosquera, M.J.; Bejarano, M.; de la Rosa-Fox, N.; Esquivias, L. Producing crack-free colloid—Polymer hybrid gels by tailoring porosity. *Langmuir* **2003**, *19*, 951–957. [CrossRef]

26. Miliani, C.; Velo-Simpson, M.L.; Scherer, G.W. Particle-modified consolidants: A study on the effect of particles on sol-gel properties and consolidation effectiveness. *J. Cult. Herit.* **2007**, *8*, 1–6. [CrossRef]

27. Salazar-Hernández, C.; Alquiza, M.J.P.; Salgado, P.; Cervantes, J. TEOS-colloidal silica-PDMS-OH hybrid formulation used for stone consolidation. *Appl. Organomet. Chem.* **2010**, *24*, 481–488. [CrossRef]

28. Liu, R.; Han, X.; Huang, X.; Li, W.; Luo, H. Preparation of three-component TEOS-based composites for stone conservation by sol-gel process. *J. Sol-Gel Sci. Technol.* **2013**, *68*, 19–30. [CrossRef]

29. Pinho, L.; Elhaddad, F.; Facio, D.S.; Mosquera, M.J. A novel TiO_2-SiO_2 nanocomposite converts a very friable stone into a self-cleaning building material. *Appl. Surf. Sci.* **2013**, *275*, 389–396. [CrossRef]

30. Karapanagiotis, I.; Pavlou, A.; Manoudis, P.N.; Aifantis, K.E. Aifantis, Water repellent ORMOSIL films for the protection of stone and other materials. *Mater. Lett.* **2014**, *131*, 276–279. [CrossRef]

31. Kronlund, D.; Bergbreiter, A.; Meierjohann, A.; Kronberg, L.; Lindén, M.; Grosso, D.; Smått, J.H. Hydrophobization of marble pore surfaces using a total immersion treatment method—Product selection and optimization of concentration and treatment time. *Prog. Org. Coat.* **2015**, *85*, 159–167. [CrossRef]

32. Colangiuli, D.; Calia, A.; Bianco, N. Novel multifunctional coatings with photocatalytic and hydrophobic properties for the preservation of the stone building heritage. *Constr. Build. Mater.* **2015**, *93*, 189–196. [CrossRef]

33. Manoudis, P.N.; Karapanagiotis, I.; Tsakalof, A.; Zuburtikudis, I.; Panayiotou, C. Superhydrophobic composite films produced on various substrates. *Langmuir* **2008**, *24*, 11225–11232. [CrossRef] [PubMed]

34. Facio, D.S.; Carrascosa, L.A.; Mosquera, M.J. Producing lasting amphiphobic building surfaces with self-cleaning properties. *Nanotechnology* **2017**, *28*, 265601. [CrossRef] [PubMed]

35. Rescic, S.; Fratini, F.; Tiano, P. On-site evaluation of the "mechanical" properties of Maastricht limestone and their relationship with the physical characteristics. *Geol. Soc. Lond. Spec. Publ.* **2010**, *331*, 203–208. [CrossRef]

36. *UNE-EN 1925:1999 Natural Stone Test Methods. Determination of Water Absorption Coefficient by Capillarity*; AENOR: Madrid, Spain, 1999.

37. Mosquera, M.J.; Benítez, D.; Perry, S.H. Pore structure in mortars applied on restoration. *Cem. Concr. Res.* **2002**, *32*, 1883–1888. [CrossRef]

38. *ASTM E 96-90 Standard Test Methods for Water Vapor Transmission of Materials*; ASTM: West Conshohocken, PA, USA, 1990.

39. Berns, R.S. *Billmeyer and Saltzman's Principles of Color Technology*; Wiley-Interscience: New York, NY, USA, 2000.

40. Ling, X.Y.; Phang, I.Y.; Vancso, G.J.; Huskens, J.; Reinhoudt, D.N. Stable and transparent superhydrophobic nanoparticle films. *Langmuir* **2009**, *25*, 3260–3263. [CrossRef] [PubMed]

41. *UNE-EN ISO 2409:2013 Paints and Varnishes. Cross-Cut Test*; AENOR: Madrid, Spain, 2013.

42. Carrascosa, L.A.; Facio, D.S.; Mosquera, M.J. Producing superhydrophobic roof tiles. *Nanotechnology* **2016**, *27*, 095604. [CrossRef] [PubMed]

43. Yu, S.; Oguchi, C.T. Role of pore size distribution in salt uptake, damage, and predicting salt susceptibility of eight types of Japanese building stones. *Eng. Geol.* **2010**, *115*, 226–236. [CrossRef]

44. Noble, K.; Seddon, A.B.; Turner, M.L.; Chevalier, P.; Mackinnon, I.A. Polysiloxane-modified mesoporous materials. *J. Sol-Gel Sci. Technol.* **2000**, *19*, 807–810. [CrossRef]

45. Della Volpe, C.; Penati, A.; Peruzzi, R.; Siboni, S.; Toniolo, L.; Colombo, C. The combined effect of roughness and heterogeneity on contact angles: the case of polymer coating for stone protection. *J. Adhes. Sci. Technol.* **2000**, *14*, 273–299. [CrossRef]

46. Cassie, A.B.D.; Baxter, S. Large contact angles of plants and animal surfaces. *Nature* **1945**, *155*, 21–22. [CrossRef]

47. Manoudis, P.N.; Karapanagiotis, I.; Tsakalof, A.; Zuburtikudis, I.; Kolinkeová, B.; Panayiotou, C. Superhydrophobic films for the protection of outdoor cultural heritage assets. *Appl. Phys. A* **2009**, *97*, 351–360. [CrossRef]

48. Pedna, A.; Pinho, L.; Frediani, P.; Mosquera, M.J. Obtaining SiO_2-fluorinated PLA bionanocomposite with application as reversible and highly-hydrophobic coatings of buildings. *Prog. Org. Coat.* **2015**, *90*, 91–100. [CrossRef]

49. Bhushan, B.; Her, E.K. Fabrication of superhydrophobic surfaces with high and low adhesion inspired from rose petal. *Langmuir* **2010**, *26*, 8207–8217. [CrossRef] [PubMed]

50. Elhaddad, F.; Carrascosa, L.A.M.; Mosquera, M.J. Long-term effectiveness, under coastal environment, of a novel conservation nanomaterial applied on sandstone from Roman archaeological site. *J. Cult. Herit.* **2018**, in press.

51. Rodrigues, J.D.; Grossi, A. Indicators and ratings for the compatibility assessment of conservation actions. *J. Cult. Herit.* **2007**, *8*, 32–43. [CrossRef]